Journal of Thermal Analysis and Calorimetry, Vol. 83 (2006) 2, 297–308

PHASE TRANSITION INDUCED BY WATER DILUTION IN PHOSPHOLIPID U-TYPE FOOD-GRADE MICROEMULSIONS STUDIED BY DSC

A. Spernath[*], *A. Aserin and N. Garti*[**]

Casali Institute of Applied Chemistry, The Institute of Chemistry, The Hebrew University of Jerusalem, Jerusalem 91904, Israel

In this study we used differential scanning calorimetry to clarify the role of water activity within the nano-droplets, and to explore phase transitions in novel phospholipids based fully dilutable food-grade microemulsions.

The microstructure transitions were investigated along two water dilution lines (50:50 and 80:20 mass% surfactant mixture/oil phase). From the water thermal behavior we learned that three structural regions can be identified along the water dilution lines. The thermal transition points coincide with the structural phase transition of the microemulsions as measured by other methods (electrical conductivity and SD-NMR measurements).

The structural transitions were detected at 20 and 45 mass% of water along dilution line 55, where along dilution line 82 it occurs at 40 and 50 mass% of water.

The microemulsions along dilution line 82 seem to have more compact surfactant packing film, thus the film has stronger resistance to transformation upon dilution, resulting in a smaller bicontinuous region than the one formed at dilution line 55. The difference in phase transition point can be used for triggering the release of future solubilizate.

Keywords: *DSC, electrical conductivity, food-grade, lecithin, microemulsions, phase-transition, phospholipids, SD-NMR*

Introduction

In recent years microemulsions have attracted the attention of many researchers as vehicles for solubilization of active molecules. The phase behavior and microstructure of those nano-sized systems have been extensively explored using a wide range of analytical techniques such as: electrical conductivity [1, 2], viscosity [1, 2], small angle X-ray scattering (SAXS) [1, 3], small angle neutron scattering (SANS) [3, 4], dynamic light scattering (DLS) [1, 5], and self-diffusion NMR [2, 6].

Differential scanning calorimetry (DSC) is very often used to study the nature of water-substrate interactions [7–10]. It is known that water departs considerably from its average bulk behavior when near solute molecules, macromolecules, colloidal particles, and solid or liquid interface [11]. A distinction between 'bulk' and 'bound' water was made. Bulk or free water is assumed to have physico-chemical properties (melting point, enthalpy, and heat capacity) similar to pure water. On the other hand, water properties differ detectably from bulk water (in some systems) as a result of the presence of a surface. Such water may be defined as 'bound' water.

DSC is regularly used for studying low-temperature behavior of water in surfactant-based multi-component microemulsion systems [12–19]. In microemulsion systems, Senatra *et al*. [20] suggested an 'operational' definition differentiating between three types of water. The differentiation is based on the difference in the water melting point since free or bulk water melts at ca. 0°C, interphasal-water melts at ca. –10°C, and bound water, which is associated with the hydrophilic head groups of the amphiphilic film, melts at <–10°C. One should note that interphasal and bound water are not always distinguishable. The water which is not detectable by the DSC is often termed 'non-freezable water' (operational, instrument-dependent definition).

Another term used in this context is water activity (a_w). Water activity [21] is defined as: $a_w=1–P/P_0$, where P is the partial pressure of water above the material and P_0 is the partial pressure of pure water at the same temperature. The term 'free water' may describe systems having a_w close to one, while the terms 'bound' and 'interphasal' may describe systems with low a_w (close to zero). Non-freezable water may describe systems having low a_w, below the detection capability of the DSC. The distinction between bound and interphasal water emphasizes the different loci of the water solubilization.

To date, DSC techniques have been used as an effective tool to investigate the temperature-induced phase transition which occurs in microemulsions systems [22, 23].

In our previous studies we presented the first generation of a U-type food-grade microemulsions system [2, 6]. These systems consisted of a mixture of

* This paper is part of Aviram Spernath's Ph.D. dissertation, The Hebrew University of Jerusalem

** Author for correspondence: garti@vms.huji.ac.il

1388–6150/$20.00
© 2006 Akadémiai Kiadó, Budapest
Akadémiai Kiadó, Budapest, Hungary
Springer, Dordrecht, The Netherlands

R(+)-limonene and ethanol as the oil phase, nonionic surfactants, and a mixture of water and propylene glycol, PG as the aqueous phase. The systems are unique, since a given composition of reverse micelles can be infinitely and progressively aqueous phase diluted with phase transition and/or morphological changes (so-called U-type systems [11]). The ability to dilute the systems to over 90 mass% of water (or aqueous phase) is important, especially for their use as carriers of nutraceuticals to produce clear beverages.

Yaghmur *et al.* [24] studied the sub-zero temperature behavior of some microemulsions based on water/PG as the aqueous phase and Tweens as emulsifiers. They found that in *w*/*o* and bicontinuous microstructures the water is either bound or interphasal. Even at high concentrations of aqueous phase, when *o*/*w* microstructures have been formed, no free water was detected, mainly because of the binding effect of the surfactants and the PG.

In this study we explored new (so-called second generation) U-type food-grade microemulsions. The new systems are superior to the first generation systems since they are free of short chain alcohol, and the surfactant mixture contains phosphatidylcholine that might have a significant role in recognizing the biomembranes for better bioadhesion and transmembrane transport.

We are presenting the use of the subzero-DSC technique as an analytical tool to characterize the nature of the water and distinguish the microstructure transitions induced by water dilution. The results were compared to findings obtained by electrical conductivity and self-diffusion NMR (PGSE NMR) measurements.

Experimental

Materials

Phospatidylcholine (Epikuron 200, PC) was obtained from Degussa Bio-Active (Hamburg, Germany). PEG-40 hydrogenated castor oil (Simulsol 1293, HECO40) was purchased from Seppic (Paris, France); PG (1,2-propanediol) was from Merck KGaA (Darmstadt, Germany); ethyl laurate (used as oil) was from Sigma Chemical Co. (St. Louis, Missouri, USA). Propionic acid was obtained from BDH (Poole, UK). All chemicals were used without further purification. The water was double distilled.

Methods

Phase diagrams

Microemulsion systems were described on pseudo-ternary phase diagrams (Fig. 1). The phase diagrams were constructed in the following way: the

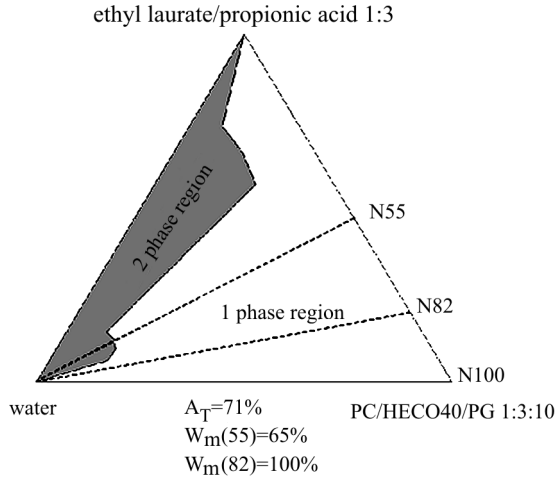

Fig. 1 Phase diagram of the second-generation, U-type, water-diluted microemulsion, at 25°C. PC – phosphatidylcholine; HECO40 – PEG-40 hydrogenated castor oil; PG – propylene glycol. Line 55 – at a surfactant mixture/oil phase ratio=50/50 and line 82 – at a surfactant mixture/oil phase ratio=80/20. A_T stands for the total isotropic area. W_m stands for the dilution capacity along specific dilution line

short-chain acid/oil mass ratio was held constant at 3:1. A stock solution of surfactant mixture containing PC/HECO40/PG at constant ratio of 1:3:10 was made. Mixtures of surfactant-oil phase were prepared in culture tubes sealed with screw caps at predetermined mass ratios of oil phase (acid plus oil) to surfactant and kept in a 25±0.3°C water bath. Microemulsion regions in phase diagrams were determined by titrating the oil-surfactant phase with water. All samples were vigorously stirred. The samples were allowed to equilibrate for at least 24 h before they were examined. In all the tested samples, evaporation loss was negligible. The different phases were determined using ocular and optical (crossed polarizers) methods. Every sample which remained transparent and homogeneous after vigorous vortexing, was considered to belong to a monophasic area in the phase diagram. The total monophasic area ($A_{T)}$ were calculated, as well as the specific dilution capacity (W_M) of each dilution line.

Calorimetric measurements

A Mettler Toledo DSC822 measuring model system was used. The instrument was calibrated every two weeks with indium, lauric acid, water, and ethyl acetate to ensure accuracy of the caloric data. The heating rate of calibration was 10 K min^{-1}. The DSC measurements were carried out as follows: 5–15 mg microemulsion samples were weighed, using a Mettler M3 microbalance, in standard 40 μL aluminum pans and immediately sealed by a press [24]; peaks representing various states of water were analyzed.

The samples were rapidly cooled in liquid nitrogen at a predetermined rate from ambient to –100°C. The sample remained at this temperature for 30 min and was then heated at 5°C min^{-1} back to ambient temperatures. An empty pan was used as a reference. The instrument determined the fusion temperatures of the solid components, and the total heat transferred in any of the observed thermal processes. The enthalpy changes associated with thermal transition were obtained by integrating the area of each pertinent DSC peak. DSC temperatures reported here were reproducible to ±0.5°C. We followed the method used by Senatra *et al.* [20] to identify various states of water in our systems, as described by Yaghmur *et al*. [24].

PGSE-NMR measurements

NMR measurements were performed on microemulsion samples at 25°C on a Bruker DRX-400 spectrometer, with BGU II gradient amplifier unit and 5 mm BBI probe equipped with a *z*-gradient coil, providing a *z*-gradient strength (*g*) of up to 55 G cm^{-1}. The self-diffusion coefficients were determined using pulsed field gradient stimulated spin-echo (BPFG-SSE) [6].

Electrical conductivity

Electrical conductivity measurements were performed at 25±1.0°C on samples using a conductivity meter, type CDM 83 (Radiometer, Copenhagen). A small amount of an aqueous electrolyte (0.01 M NaCl solution) must be added for electrical conduction. It should be noted that the samples containing the salt remained clear upon dilution or storage and there were no observable changes in the phase diagram. Similar independence of phase behavior in the presence of a small amount of electrolyte has been reported in the literature [25, 26].

Results and discussion

Phase diagrams

The pseudo-ternary phase diagram of the second-generation, U-type, food-grade microemulsion system composed of ethyl laurate/propionic acid/PC/H-ECO40/PG is shown in Fig. 1. All measurements were made along dilution lines 55 (50 mass% surfactants and 50 mass% oil phase) and 82 (80 mass% surfactants and 20 mass% oil phase).

It was found that U-type systems can be made even in the absence of short chain alcohol, if the surfactant mixture contains PC and hydrophilic nonionic surfactant (H-ECO40). Instead of short chain alcohol, we used propionic acid as cosurfactant. The propionic acid provides a low pH which might be beneficial for clear beverages. The one-phase region area (A_T) is 71% of the total phase diagram. The dilution capacity of water along dilution line 55 (W_m) is 65 mass% while the W_m along dilution line 82 is 100% (dilution to infinity, Fig. 1).

DSC measurements

Dilution of the surfactants/PG mixture with oil phase and water

The melting temperatures of the individual microemulsion ingredients are summarized in Table 1. The thermal behavior of both the surfactants and the oil phase were examined separately. The mixture of ethyl laurate and propionic acid forms an isotropic solution with distinct one endothermic event at –24.0°C (ΔH_f=–162.5 J g^{-1}) (Fig. 2a). The blend of the three ingredients that compose the surfactant phase (PC, HECO40, and PG) also forms a molecular mixture (complex or hybrid or molecular structure with strong interactions) that melts at 7.0°C (ΔH_f=–18.7 J g^{-1}) (peak A, Fig. 2b). A minor endothermic event also occurs at –24.0°C (ΔH_f=–1.0 J g^{-1}) (peak B). However, this mixture is strongly affected by water or oil. A typical curve of a 20 mass% water microemulsion at N55 dilution line is shown in Fig. 2c.

Table 1 Melting temperature of the microemulsion components

Component	Melting temp./°C
Ethyl laurate	1.0[a]
Propionic acid	–21.0[a]
Phosphatidylcholine (Epikuron 200)	36.0[a]
PEG-40 hydrogenated castor oil	36.0[a]
Propylene glycol	–59.0[b]

[a]Melting temperatures as measured by the DSC,
[b]Melting temperature taken from the literature [27]

Addition of the oil phase to the surfactants/PG mixture (Fig. 3a) destabilizes the molecular mixture of the surfactants and affects the molecular balance between the head groups of the surfactants and the PG, and the hydrophobic interaction between the tails. As a result, the endothermic peak A which represents the melting of the 'molecular complex' splits into two endothermic events (peaks A and A1 in Table 2). Melting also shifts to lower temperatures and its ΔH_f decreases (Table 2). This means that the molecular bond between the surfactants and the PG weakens; the surfactant gains more mobility and defrosts at lower melting points. Peak B in Fig. 3 appears at similar melting range (20.0±2°C), and its ΔH_f remains almost unchanged (Table 2). As the content of the oil phase increases, interactions between the molecular complexes of the surfactants-PG are weakened, and the individual

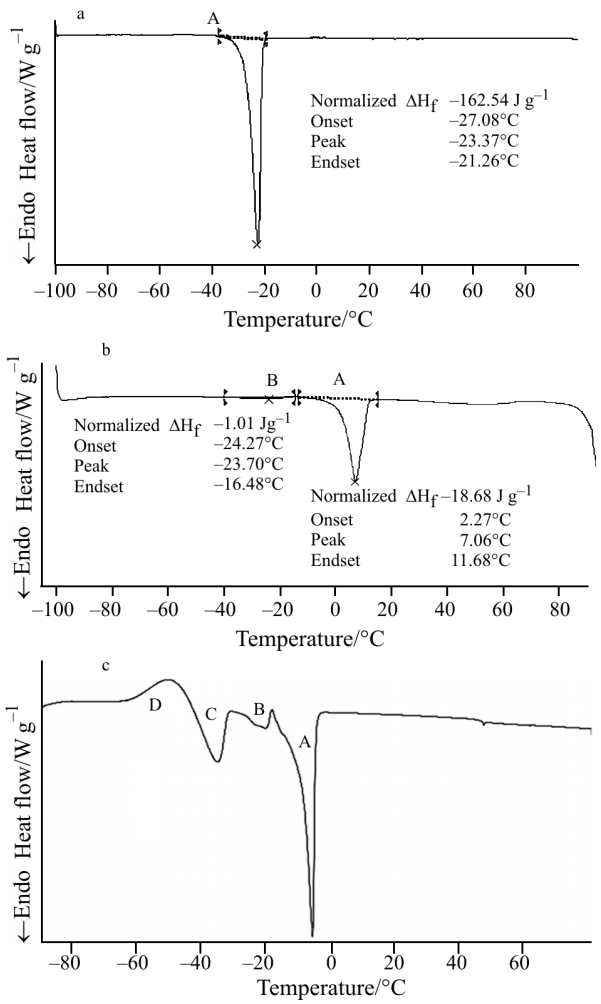

Fig. 2 DSC curves of a – oil phase containing ethyl laurate and propionic acid at a mass ratio of 1:3 respectively; b – surfactant mixture containing phosphatidylcholine, HECO40, and propylene glycol at a mass ratio of 1:3:10 respectively; c – typical microemulsion contains ethyl laurate and propionic acid at a 1:3 ratio as the oil phase; PC, HECO40 and PG at a ratio of 1:3:10 as surfactants mixture and water. Peaks A and B relates to the fusion of the surfactants mixture, peak c relates to water fusion, and peak d relates to water molecules rearrangement

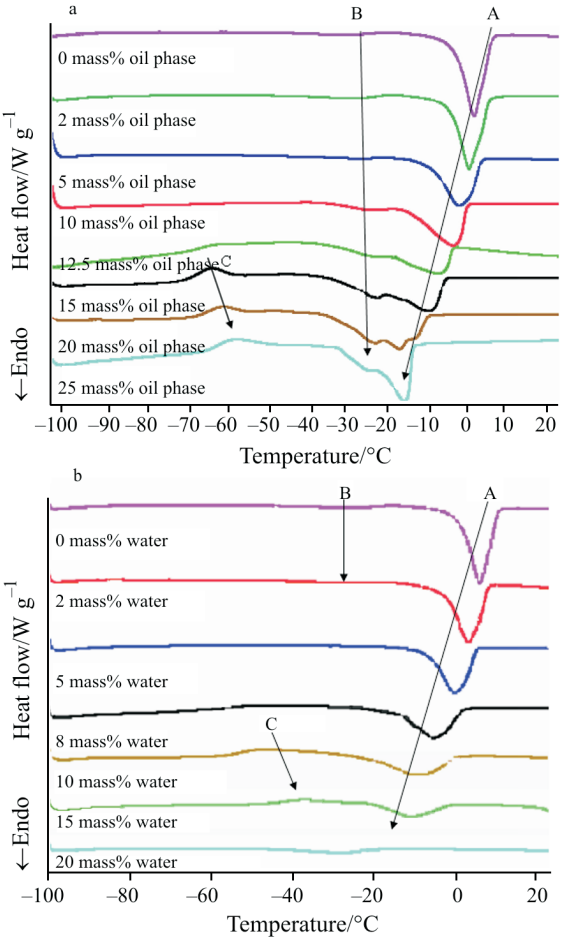

Fig. 3 DSC curves of a – surfactant mixture diluted by the oil phase; b – surfactant mixture diluted by water (dilution line N100)

components melt as separate entities. Those melting temperatures of the individual entities may be different from their pure melting points as the melting temperature of confined substance is substantially different from its bulk melting point. Finally, a new exothermic event appears at ca. –56°C (peak D) in systems containing 15–20 mass% oil phase, which split into two exothermic events (peak C at –42.5°C and peak D at –56.0°C) in system with 20 mass% of water (Table 2).

Adding water to the surfactants/PG mixture (dilution line N100, Fig. 1), forces the major endothermic event (peak A), of the surfactants/PG mixture, to appear at lower temperature (Fig. 3b). The melting temperature of the surfactant mixture diluted with 20 mass% water decreases substantially from 7.0°C to –27.4°C (Table 2). At the same time, the ΔH_f values of both the major and the minor endothermic events (peaks A and B) decrease as more water is incorporated. Peak B disappears in a system containing 5 mass% of water. It seems that the water molecules destabilize the structure of the surfactant mixture, and decrease its melting temperature and ΔH_f. The water causes peak A to split (peaks A and A1 in Table 2) while a new exothermic event occurs at ca. –46°C (peak C, Table 2) in systems with 10 and 15 mass% water.

It seems that the introduction of a small amount of water or oil phase (up to 20 mass%) to the surfactant mixture causes the formation of weaker complexes, thus the major endothermic events appear at lower temperatures. The exothermic events that appear when the surfactant mixture dilutes with oil phase or water are not yet fully resolved. However, we can say that those exothermic events occur only at intermediate stages and disappear upon adding more water or more oil phase.

Table 2 Thermal behavior of surfactants/PG mixture diluted with water or oil phase, measured by DSC

	Dilution/ mass%	Peak A		Peak A1		Peak B		Peak C		Peak D	
		T/°C	ΔH_f/J g^{-1}	T/°C	ΔH_f/J g^{-1}	T/°C	ΔH_f/J g^{-1}	T/°C	ΔH_f/J g^{-1}	T/°C	ΔH_f/J g^{-1}
No dilution	–	7.0	–18.7	–	–	–23.7	–1.0	–	–	–	–
Oil phase diluted	2	5.8	–17.9	–	–	–23.5	–1.9	–	–	–	–
	5	2.2	–15.3	–	–	–23.0	–0.5	–	–	–	–
	10	0.7	–13.3	–	–	–20.6	–0.8	–	–	–	–
	12.5	–2.0	–15.1	–	–	–19.4	–0.8	–	–	–	–
	15	–4.2	–18.4	–11.6	–0.1	–18.7	–1.4	–	–	–58.5	2.6
	20	–7.0	–0.7	–11.5	–16.9	–18.5	–1.3	–42.5	0.4	–56.0	2.1
	25	–6.5	–0.01	–10.7	–18.5	–20.6	–1.1	–33.6	0.1	–52.9	3.2
Water diluted	2	4.2	–16.7	–	–	–22.9	–0.5	–	–	–	–
	5	0.8	–14.8	–	–	–	–	–	–	–	–
	8	–4.3	13.5	–9.2	–0.1	–	–	–	–	–	–
	10	–7.1	–13.7	–10.9	–0.3	–	–	–46.5	3.3	–	–
	15	–9.9	–5.7	–	–	–	–	–35.9	1.4	–	–
	20	–27.4	–2.6	–	–	–	–	–	–	–	–

It seems clear that the thermal events that were recorded at low water and low oil contents are related to the surfactant mixture reorganization in the presence of water or oil.

In a system containing 50 mass% surfactant mixture and 50 mass% oil phase (line N55, without water, Table 3), two endothermic events appear. The first, at –12.7°C, seems to be related to the surfactant mixture, while the second at –24.4°C, seems to be related to the oil phase. This endothermic event can not be attributed to the surfactant phase, as in systems containing up to 20 mass% oil phase, because it appears at a lower temperature. After attributing the endothermic peaks to the surfactant behavior, we examined dilution lines 55 and 82 in more detail.

Dilution line 55

Table 3 shows that at any water content up to 15 mass%, two endothermic events are detected; at –12.7 to –7.6°C (peak A) and at –23.0±2°C (peak B). Those two events correlate with the fusion of the molecular mixture of the oil phase and the surfactant mixture, respectively as determined above. In system containing 17 mass% of water, a third peak (peak C) appears at –42.2°C. Peak C may be related to the appearance of bound-water. Peak A moves slightly to higher temperature (from –12.7 to –7.6°C) as the water concentration increases, while peak B remains virtually unchanged. Moreover, the ΔH_f of peaks A and B remain almost unchanged (Table 3). It can be expected that addition of water will cause peak A to move to lower temperatures as in the case of dilution line N100, that was previously discussed, but in a system containing 50 mass% oil phase, the addition of water increases the order in the system as reverse micelles start to appear. It should be noted that in this region no explicit water related endothermic events are detected (except to minor amounts of bound water in a system containing 17 mass% water). This means that the water activity is below the identification capability of the DSC technique. We termed this type of water 'non-freezable water' or 'non-detectable' water.

Figure 4 shows endothermic and exothermic events occurring in microemulsion systems containing 20–50 mass% water along dilution line 55. New endothermic events (peak C) were registered at –42.2±1.0°C, in microemulsions containing 17 mass% water (Table 1) (because of its small ΔH_f (–0.19 J g^{-1}) it is not shown in Fig. 4). The ΔH_f of peak C increases as the water concentration increases from 6.7 J g^{-1}, at 20 mass% water, to 71.08 J g^{-1} at 50 mass% water (Table 3). The enthalpic values suggest that peak C should be attributed to fusion of water. For further identification of peak C, we prepared microemulsion samples in which

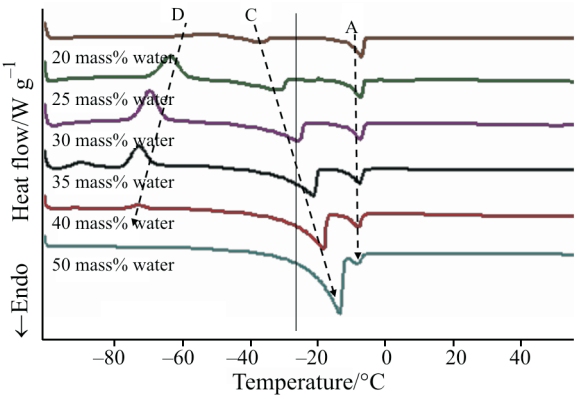

Fig. 4 DSC curves of microemulsions along dilution line 55 (20–50 mass% water) containing ethyl laurate and propionic acid at a 1:3 ratio as the oil phase; PC, HECO40 and PG at a ratio of 1:3:10 as the surfactant mixture

Table 3 Thermal behavior of the microemulsion system along the one-phase region at dilution line 55 at different water concentrations measured by DSC

Water*/mass%	Peak A[a]		Peak B[a]		Peak C[b]		Peak D[c]	
	T/°C	ΔH_f/J g^{-1}	T/°C	ΔH_f/J g^{-1}	T/°C	ΔH_f/J g^{-1}	T/°C	ΔH_f/J g^{-1}
0	–12.7	–8.20	–24.4	–0.59	–	–	–	–
5	–10.6	–10.25	–22.7	–1.84	–	–	–	–
10	–8.8	–12.93	–22.5	–1.70	–	–	–	–
15	–7.6	–9.38	–22.0	–1.93	–	–	–	–
17	–7.4	–14.95	–21.8	–2.00	–42.2	–0.19		
20	–7.8	–13.90	–22.3	–1.48	–37.5	–6.70	–52.7	5.35
25	–8.0	–9.81	–21.6	–0.90	–31.4	–14.63	–63.3	24.15
30	–8.0	–10.23	–21.3	0.19	–26.3	–24.16	–69.7	26.82
35	–8.3	–8.14	–	–	–21.7	–33.46	–72.7	18.02
40	–8.6	–7.36	–	–	–18.8	–41.96	–72.9	1.96
50	–8.9	–1.98	–	–	–14.0	–71.08	–	–
55	–	–	–	–	–11.4	–114.4	–	–
60	–	–	–	–	–9.9	–117.8	–	–
65	–	–	–	–	–8.3	–139.9	–	–

*Along dilution line 55, the isotropic region exists only up to 65 mass% water, [a]peaks were interpreted as the melting point of the surfactant mixture, [b]peak was interpreted as the melting point of water, [c]peak was interpreted as the recrystallization of bound-water

the water was replaced by D_2O (containing 30 and 65 mass% D_2O). Typical shift of ca. +4°C was detected, in both systems, for peak C in a microemulsion containing D_2O, which confirms that peak C is an endothermic event related to the fusion of water. The shift was not detected for peaks A and B, confirming that the endothermic events of peaks A and B are not water-related. The low melting points of water in those systems (–37.5°C at 20 mass% water, up to –14.0°C at 50 mass% water) suggest that the water is bound. One should note that in a system containing 50 mass% water, peak B is not detectable (possibly because of the dilution effect).

An exothermic event (peak D) is detected only in systems containing 20–40 mass% water (Fig. 4). The identification of peak D as a water-related event was made possible as a shift of ca. 4°C was detected when water was replaced by D_2O. The temperature of the exothermic events is lower as the water concentration increases (from –52.7°C at 20 mass% water to –72.9°C at 40 mass% water). The ΔH_f of peak D goes through a maximum at 30 mass% of water (ΔH_f=26.82 J g^{-1}). In a system containing 40 mass% water, peak D is very small (ΔH_f=1.96 J g^{-1}), while in a system containing 50 mass% water, no exothermic event occurs.

As we could see from the endothermic events, at low water content most of the water is non-freezable or undetectable. As the water content increases, the mobility and activity of the water increases and the non-freezable water rearranges at –60 to –70°C to become bound (rather than non-freezable). Such rearrangement seems to be similar to a crystallization event which is detected as an exothermic event. At 50 mass% water, there are sufficient quantities of water with high mobility and high activity, so such re-crystallization is not observed or detected.

It can be seen from Fig. 5 that once the water content exceeds 50 mass%, only peak C appears. The fact that no other endothermic events are detected is related to the fact that upon high dilution, the detectability of the other events becomes impossible (dilution factor). The water melting-points in this region are between –14.0°C at 50 mass% to –8.3°C at 65 mass% water. This suggests that the water is slowly transferred from

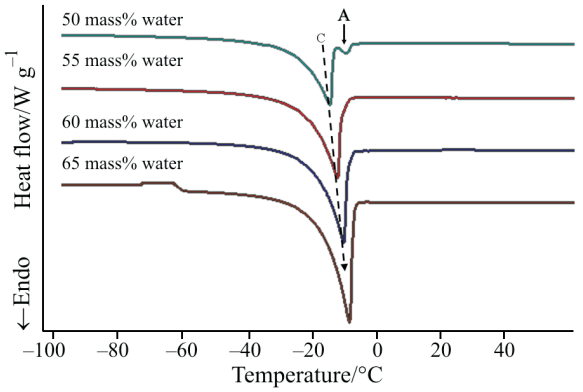

Fig. 5 DSC curves of microemulsions along dilution line 55 (50–65 mass% of water) containing ethyl laurate and propionic acid at a 1:3 ratio as the oil phase; PC, HECO40 and PG at a ratio of 1:3:10 as the surfactant mixture

bound water into interphasal water or, alternatively the water is more loosely bound to the surfactants.

The equations used by Senatra *et al*. [20] and Yaghmur *et al.* [24] to identify various states of water were applied and it was clearly seen (Fig. 6) that in systems containing 0–15 mass% water, all the water was non-freezable, as all water molecules are bound to the surfactant head groups. In a system containing 17 mass% water (Table 3) one could detect, for the first time, a very small amount of bound-water (0.36 mass% of the water is bound-water). In systems containing 20–40 mass% water, the concentration of non-freezable water decreased continuously from 89 to 66 mass% of the total water added, and the concentration of bound water increases from 10 up to 34 mass%. The decrease in non-freezable water content may be due to the saturation by the amphiphilic film of the water molecules, thus the excess of water molecules with high activity are poorly accommodated at the amphiphilic film and they become free as part of the continuous phase. Further increase in water concentration in the microemulsion systems (up to 65 mass% water) causes a further decrease in the non-freezable water concentration (from 55 to 31 mass%). Furthermore, the amounts of high-activity water (up to 69 mass%) increases. The activity of the water seems to be higher than the activity of the bound water, thus we termed it 'interphasal water'. Further increase in water

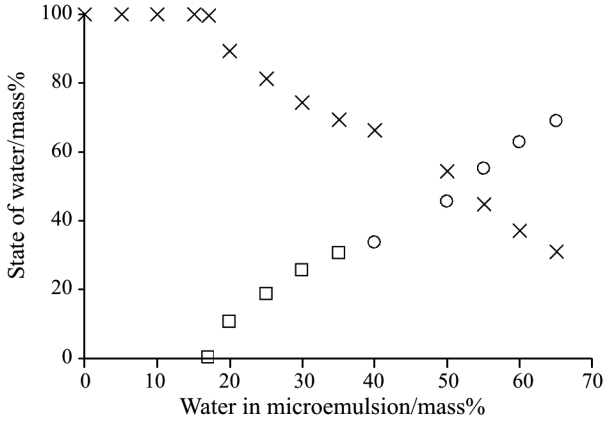

Fig. 6 Variation in the content of × – non-freezable, ○ – interphasal and □ – bound-water as a function of water concentration along dilution line 55. Phase separation occurs above 65 mass% water

concentration along this dilution line causes breakdown of the microemulsion, and phase separation.

From Table 3 and Figs 4 and 5, it can be seen that dilution line 55 can be divided into three regions. In the first region (0–15 mass% water) no water-related endotherms occur. In the second region (17–40 mass%), water related exotherms and endotherms appear. In the third region (50–65 mass%) only one, big endothermic event of bound water is detected.

Dilution line 82

Dilution line 82 (80 mass% surfactants and 20 mass% oil phase) was investigated similarly. One can see from Figs 7, 8 and Table 4 that the general behavior is similar to that of dilution line 55. The three main regions are within 0–35, 40–50 and 55–95 mass% water.

In the first region (0–35 mass% water), as in dilution line 55, no water related events were detected (peak C, Table 4). The endothermic events recorded in this region are correlated only to the surfactant mixture.

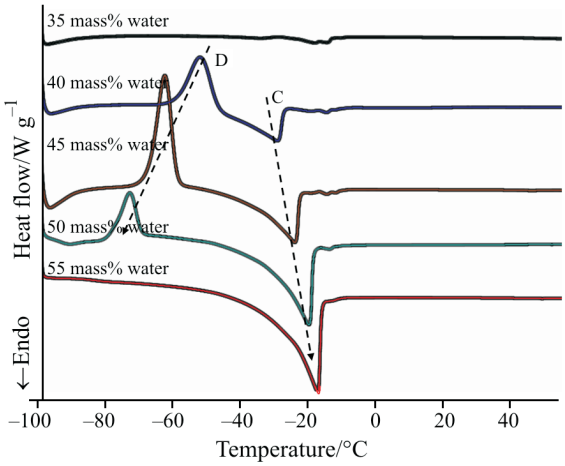

Fig. 7 DSC curves of microemulsions along dilution line 82 (35–55 mass% water) containing ethyl laurate and propionic acid at a 1:3 ratio as the oil phase; PC, HECO40 and PG at a ratio of 1:3:10 as the surfactant mixture

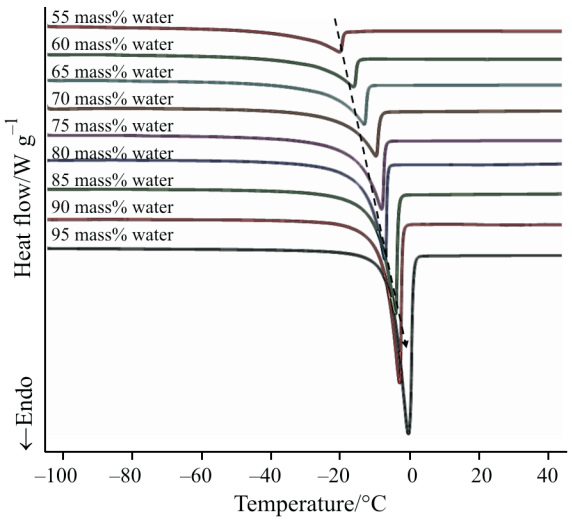

Fig. 8 DSC curves of microemulsions along dilution line 82 (55–95 mass% of water) containing ethyl laurate and propionic acid at a 1:3 ratio as the oil phase; PC, HECO40 and PG at a ratio of 1:3:10 as the surfactant mixture

Table 4 Thermal behavior of microemulsions along dilution line 82 at different water concentrations (measured by DSC)

Water/mass%	Peak A[a]		Peak A1[a]		Peak B[a]		Peak C[b]		Peak D[c]	
	T/°C	ΔH_f/J g^{-1}	T/°C	ΔH_f/J g^{-1}	T/°C	ΔH_f/J g^{-1}	T/°C	ΔH_f/J g^{-1}	T/°C	ΔH_f/J g^{-1}
0	–11.5	–0.94	–18.5	–1.33	–	–	–	–	–	–
5	–10.6	–1.24	–16.8	–0.43	–25.8	–3.06	–	–	–	–
10	–10.0	–0.93	–16.1	–0.48	–25.9	–1.84	–	–	–	–
15	–9.6	–0.85	–15.4	–0.46	–25.8	–1.59	–	–	–	–
20	–8.8	–1.14	–15.8	–0.78	–23.6	–0.07	–	–	–	–
25	–9.0	–0.58	–15.6	–1.72	–	–	–	–	–	–
30	–	–	–14.3	–0.51	–	–	–	–	–	–
35	–	–	–13.8	–0.53	–	–	–	–	–	–
40	–	–	–14.2	–0.40	–	–	–29.0	–29.86	–52.1	27.24
45	–	–	–14.1	–0.34	–	–	–23.9	–42.91	–62.8	49.97
50	–	–	–13.2	–0.39	–	–	–19.6	–66.31	–73.4	20.75
55	–	–	–	–	–	–	–17.0	–89.98	–	–
60	–	–	–	–	–	–	–13.0	–91.08	–	–
65	–	–	–	–	–	–	–10.2	–116.03	–	–
70	–	–	–	–	–	–	–6.9	–130.52	–	–
75	–	–	–	–	–	–	–5.4	–167.15	–	–
80	–	–	–	–	–	–	–3.7	–199.58	–	–
85	–	–	–	–	–	–	–1.8	–221.57	–	–
90	–	–	–	–	–	–	–1.1	–253.11	–	–
95	–	–	–	–	–	–	1.2	–312.47	–	–

[a]Peaks were interpreted as the melting point of the surfactant mixture, [b]peak C was interpreted as the melting point of water and [c]peak D was interpreted as the recrystallization of bound-water

The addition of water along this dilution line causes an endothermic splitting. The peak splitting may indicate the influence of added water to the surfactant mixture.

In the second region (40–50 mass% water), water related endothermic and exothermic events appeared (peaks C and D; Fig. 7). As in dilution line 55, the identification of those events as water-related was made by replacing the water with D_2O. As one can see in Table 4, the ΔH_f of peak D runs through a maximum (49.97 J g^{-1}) in a system containing 45 mass% water, and the peak temperature decreases from –52.1°C in a system containing 40 mass% water, to –73.4°C in a system containing 50 mass% water. At higher water concentrations the exothermic event is not detected.

The endothermic water-related event (peak C) also appears in a system containing 40 mass% water (Fig. 7). The absolute ΔH_f of peak C increases from 29.86 J g^{-1} in a system containing 40 mass% water to 89.98 J g^{-1} in system containing 55 mass% water. Peak temperature increases from –29 to –17°C, respectively.

In the third region, shown in Fig. 8, only water-related endotherms appear (peak C). The ΔH_f of peak C increases as the water concentration increases from 50 to 95 mass% water (ΔH_f at 55 mass% water is 89.98 J g^{-1}, and at 95 mass% water the ΔH_f is 312.5 J g^{-1}, Table 4). The temperature of these endothermic events gradually increases from –17°C at 55 mass% water to 1.2°C at 95 mass% water. The bound-water progressively becomes interphasal water and finally turns to free water once *o*/*w* microemulsions are formed.

From Table 4 and Figs 7 and 8 one can postulate that all the water in the first region has very low activity and is undetected by the DSC instrument. This indicates that the water in this region (Table 4) is confined and strongly bound inside the microstructure of the *w*/*o* microemulsion. In the second region (Fig. 7), appearance of the water-related event (peak C) suggests that at least part of the water has a higher activity and is detected by the DSC. The temperatures of the endothermic peak (–29°C at 40 mass% water, and –19.6°C at 50 mass% water) suggests that the water molecules are associated with the hydrophilic parts of the amphiphilic molecules. In the third region (Fig. 8), a progressive increase in the water melting (peak C), suggests that the water molecules have increased activity. In systems containing between 60–75 mass% water, peak C appears between –13 to –5.4°C suggesting that the water molecules are still somewhat confined within the interface of the dispersed phase. We termed them ‘interphasal-water’. At

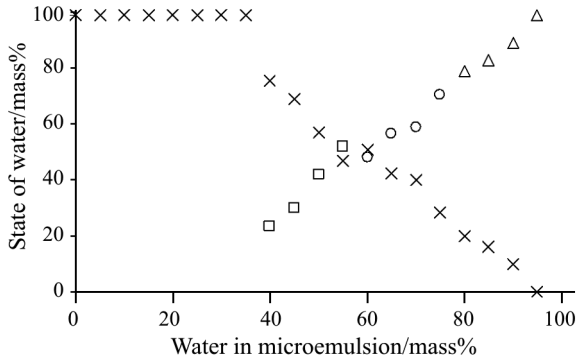

Fig. 9 Variation in the content of × – non-freezable, o – interphasal, □ – bound Δ – and free-water as function of water concentration along dilution line 82

higher water concentrations (over 75 mass%) water in the microemulsions seems to be free water, as the ΔH_f approaches the ΔH_f of pure water.

Similarly to dilution line 55, the exotherm appearing along dilution line 82 in microemulsion systems containing 40–50 mass% of water may be related to the reorganization of the water molecules.

As per Senatra's equations, the non-freezable water concentration decreases continuously as the total water concentration increases (Fig. 9). In systems containing up to 40 mass% water, all the water is non-freezable. At water content of 40–55 mass% the water is bound, while in systems with 60–75 mass%, interphasal-water is seen. At the high-dilution ends of 80–90 mass% water, the water is mostly free, while in microemulsions containing 95 mass% water, the water is completely free.

The DSC results show that in the second generation of microemulsions along both dilution lines the bound and interphasal water do not coexist. In the first generation microemulsions [24], a) bound and interphasal-water were found to coexist, while no free-water was found, even at high water concentrations, b) the surfactant-oil mixtures were diluted with a mixture of water and propylene glycol (PG). Thus, even at a high concentration of aqueous phase, the water molecules were always bound to the PG molecules, which are strongly hydrated by water. In our new systems the dilution is made with water alone, thus at high water content (over 90 mass% water along dilution line 82) the water molecules are completely free. In addition, the coexistence of bound and interphasal water in Yaghmur's [24] microemulsions seems to indicate that the surfactant molecules are loosely packed, in contrast to the system investigated in this study. In our present system the nature of the surfactants dictates tight film packing in the *w*/*o* region, resulting in mostly non-freezable and bound water but once inversion occurs (to *o*/*w*), the water becomes free.

From Table 4, Figs 7 and 8 along dilution line 82 one can see that the three regions are distributed slightly differently as compared with systems with lower surfactant concentration (line 82 *vs*. line 55): 0–40 mass% water (1st region), 40–50 mass% water (2nd region), and over 55 mass% water (3rd region).

When comparing the two dilution lines (lines 55 and 82) one can see that the bicontinuous region (the second region) is narrower for dilution line 82 than for dilution line 55, and the *w*/*o* microemulsion restructures at a higher water concentration. The bicontinuous microstructure contains a local inflection point in the surfactant film curvature, thus the film has to be flexible. Dilution line 82 is more saturated with surfactant and contains a decreased concentration of co-surfactant (propionic acid) compared with dilution line 55. Thus, the surfactant film along dilution line 82 is more tightly packed and has a lesser tendency to form a bicontinuous structure.

Two other analytical methods were employed to strengthen our structural transition assumptions.

Electrical conductivity and self-diffusion coefficient

The ability of electrical conductivity and PGSE NMR (Self Diffusion-NMR, SD-NMR) techniques to identify phase transition in microemulsion systems is well documented in the literature [2, 6, 28]. In this work we both measured the electrical conductivity (Fig. 10)

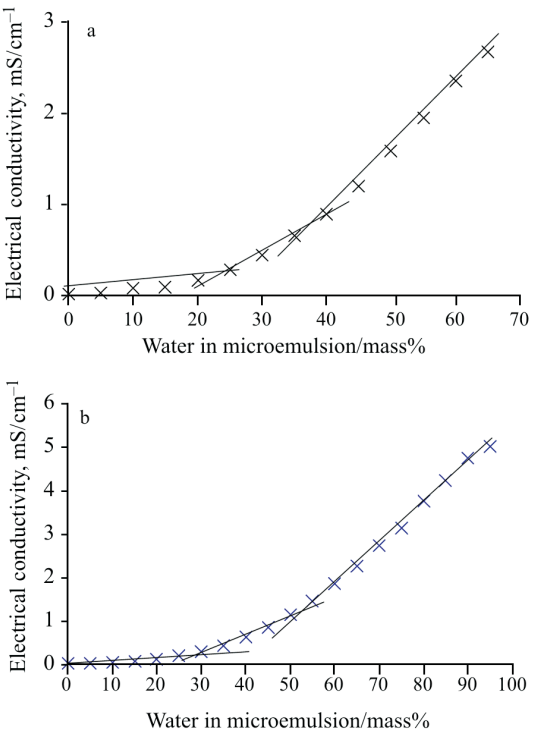

Fig. 10 Electrical conductivity at 25°C of microemulsions along a – dilution line 55 and b – dilution line 82 containing ethyl laurate and propionic acid at a 1:3 ratio as the oil phase; PC, HECO40 and PG at a ratio of 1:3:10 as the surfactant mixture

and determined changes in diffusion coefficients (Figs 11 and 12) along dilution lines 55 and 82.

From Figs 10a and b one can see changes in the slopes of the conductivity curves indicating microstructural transition. The first transition along dilution line 55 (Fig. 10a) occurs at ca. 20 mass% water, and the second transition takes place at ca. 40 mass% water. Over 65 mass% water micro-emulsification failure occurs. Along dilution line 82 (Fig. 10b), the transitions occur at ca. 30 and 50 mass% water. The microstructure is gradually inverted from *w*/*o* to bicontinuous, and from bicontinuous into an *o*/*w* microemulsion.

There is a slight difference in the transition point as one follows dilution line 55 or dilution line 82. The bicontinuous region along dilution line 82 (second region) narrows and occurs at a higher water concentration than in dilution line 55.

Plotting the diffusion coefficient (DC) of water and ethyl laurate (Figs 11, 12, respectively) *vs*. water concentration along the two dilution line shows three different regions. The transition points were identified by changes in the slope of the diffusion curve.

Along dilution line 55 (Fig. 12a) one can see from the ethyl laurate DC curve the transition points from *w*/*o* to bicontinuous structure at ca. 20 mass% water, while the transition is not detected on the water DC curve (Fig. 11a). The bicontinuous transformation to *o*/*w* detected on both the water and ethyl laurate DC curves (Figs 11a and 12a) and occurs at ca. 50 mass% water.

Figures 11b and 12b shows the DC curves of water and ethyl laurate along dilution line 82. The general behavior is similar to the behavior along dilution line 55, but the transition points are different. The transition from *w*/*o* to bicontinuous structure occurs at ca. 40 mass% water, while the transition from bicontinuous

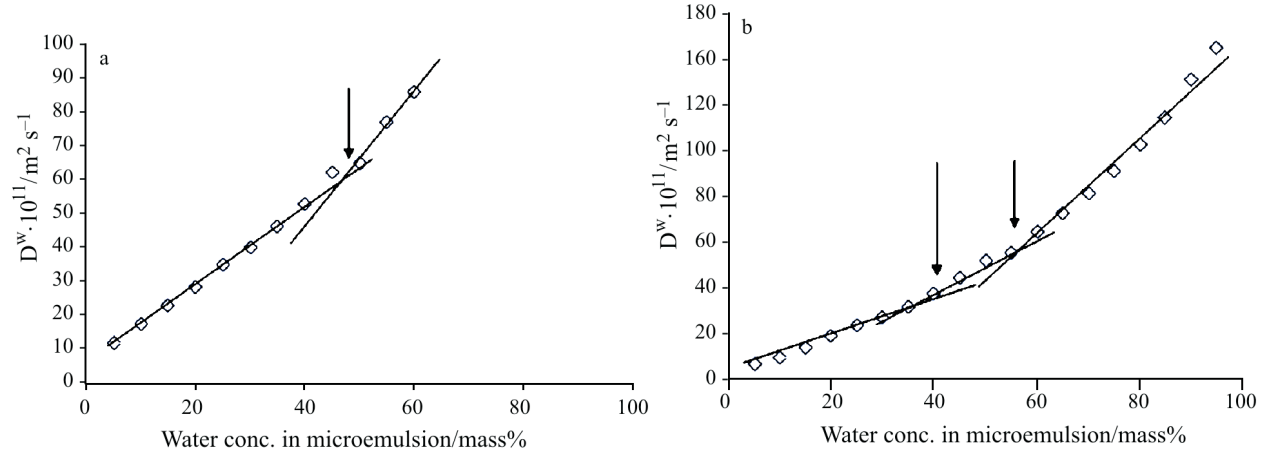

Fig. 11 Diffusion coefficients at 25°C obtained from SD-NMR measurements of a – water along dilution line 55, b – water along dilution line 82 The microemulsions contain ethyl laurate and propionic acid at a 1:3 ratio as the oil phase; PC, HECO40 and PG at a ratio of 1:3:10 as the surfactant mixture

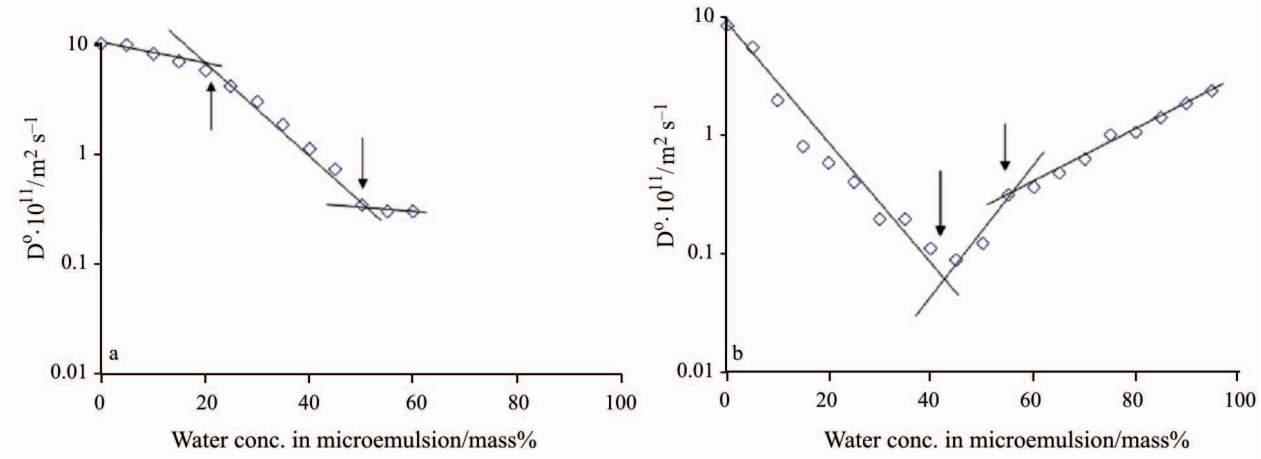

Fig. 12 Diffusion coefficients at 25°C obtained from SD-NMR measurements of a – ethyl laurate along dilution line 55, b – ethyl laurate along dilution line 82. The microemulsions contain ethyl laurate and propionic acid at a 1:3 ratio as the oil phase; PC, HECO40 and PG at a ratio of 1:3:10 as the surfactant mixture

Table 5 Transition regions along dilution lines 55 and 82 obtained from different analytical methods

Dilution line	Method	Microstructure regions/mass% water		
		w/*o*	bicontinuous	*o*/*w*
Line 55[a]	DSC	0–25	30–40	50–65
	SD-NMR	0–25	30–40	50–65
	electrical conductivity	0–20	25–45	50–65
Line 82[b]	DSC	0–35	40–50	>50
	SD-NMR	0–40	45–55	>55
	electrical conductivity	0–30	35–50	>50

[a]All compositions contain 50 mass% oil phase and 50 mass% surfactants, [b]all compositions contain 20 mass% oil phase and 80 mass% surfactants

to *o*/*w* structure occurs at ca. 50 mass% water. As in dilution line 55, the transition points are more pronounced with the ethyl laurate DC curve (Fig. 12b).

The water DC curve (Fig. 11) seems to be less affected by the structural transition as the water is slowly and progressively covert from being the inner-phase (*w*/*o*) to become the continuous phase (*o*/*w*) as represent by DSC results.

One can see that DC behavior of ethyl laurate along line 55 (Fig. 12a) differ from the DC behavior along line 82 (Fig. 12b). DC along line 55 is progressively decreased (as expected when the system covert from *w*/*o* to *o*/*w* microstructure), while along line 82 the DC decreases when the system contains less than 40 mass% of water and increase as the water concentration exceeded above 40 mass% of water. We can't receive diffusion coefficient above 65 mass% of water along line 55 as the system along this dilution line can only be diluted up to 65 mass% of water without phase separation.

In Table 5 we summarize the microstructure transition as reflected from the three different analytical techniques. One can see that there is good agreement between the three different analytical techniques (DSC, electrical conductivity, SD-NMR) in regard to the microstructure transition points.

Conclusions

DSC measurements are a quantitative tool to evaluate the level of mobility and activity of the water molecules as a function of surfactant concentration and dilution with water (dilution line 55 and 82) in any microemulsion, including more complex second-generation microemulsions. When the activity of water is below the detection ability of the DSC (non-freezable water), all water molecules are confined to the water core of the reverse micelles. As the water content increases, the water gains mobility, transforms into bicontinuous, and finally turns into free water when the microemulsion become *o*/*w*.

The difference in the transition points between the dilution lines may affect the capacity and stability of any water-soluble solubilizates. As water molecules are more confined into the core of the micelles, the solubilizate is better protected, thus is more stable. One can also use the difference in the transition point between lines 55 and 82 for triggering the release of a solubilizate.

Sub-zero DSC can be used to detect the phase transition points of food-grade U-type microemulsions. The result measurements are in good agreement with those obtained from electrical conductivity and SD-NMR techniques. SD-NMR is expensive, and very difficult to measure and to interpret technique. DSC, along with conductivity measurements, can be considered as extremely simple and reliable technique. Those combined techniques can determine water mobility and activity along with structural transitions of any U-type microemulsions that are complex systems in composition and structure.

Acknowledgements

The authors wish to thank to Dr. Roy E. Hoffman, from the Department of Organic Chemistry at the Hebrew University of Jerusalem, for his contribution to this study. The authors will also wish to thank NutraLease Ltd. for their generous financial support.

References

1 F. Podlogar, M. Gašperlin, M. Tomšič, A. Jamnik and M. B. Rogač, Int. J. Pharm., 276 (2004) 115.
2 A. Yaghmur, A. Aserin, B. Antalek and N. Garti, Langmuir, 19 (2003) 1063.
3 O. Regev, S. Ezrahi, A. Aserin, N. Garti, E. Wachtel, E. W. Kaler, A. Khan and Y. Talmon, Langmuir, 12 (1996) 668.
4 L. de Campo, A. Yaghmur, N. Garti, M. E. Leser, B. Folmer and O. Glatter, J. Colloid Interface Sci., 274 (2004) 251.
5 M. Tomšič, M. B. Rogač, A. Jamnik, W. Kunz, D. Touraud, A. Bergmann and O. Glatter, J. Phys. Chem. B, 108 (2004) 7021.

6 N. Garti, A. Aserin, S. Ezrahi, I. Tiunova and G. Berkovic, J. Colloid Interface Sci., 178 (1996) 60.
7 K. Cieśla, H. Rahier and G. Zakrzeewska-Trznadel, J. Therm. Anal. Cal., 77 (2004) 279.
8 K. Tananuwong and D. S. Reid, J. Agric. Food Chem., 52 (2004) 4308.
9 A. Raemy, J. Therm. Anal. Cal., 71 (2003) 273.
10 J. F. A. Soltero, J. E. Puig and P. C. Schulz, J. Thermal Anal., 51 (1998) 105.
11 A. Spernath, A. Yaghmur, A. Aserin, R. E. Hoffman and N. Garti, J. Agric. Food Sci., 51 (2003) 2359.
12 J. Koetz, J. Bahnenann and S. Kosmella, J. Polym. Sci. Pol. Chem., 42 (2004) 742.
13 G. Xu, L. Zhang, S. Yuan, X. Huang and G. Li, J. Dispersion Sci. Technol., 22 (2001) 563.
14 P. C. Schulz, J. Thermal Anal., 51 (1998) 135.
15 D. Clausse, J. Thermal Anal., 51 (1998) 191.
16 D. Vollmer, J. Vollmer, R. Strey, H. G. Schmidt and G. Wolf, J. Thermal Anal., 51 (1998) 9.
17 K. Cieśla, H. Rahier and G. Zakrzewska-Trznadel, J. Therm. Anal. Cal., 77 (2004) 279.
18 N. Zajc and S. Srcic, J. Therm. Anal. Cal., 77 (2004) 571.
19 A. Raemy, C. A. Nouzille, P. Frossard, L. Sagalowicz and M. E. Leser, J. Therm. Anal. Cal., 80 (2005) 439.
20 D. Senatra, L. Lendinara and M. G. Giri, Prog. Coll. Polym. Sci., 84 (1991) 122.
21 V. Kocherbitov, Thermochim. Acta, 414 (2004) 43.
22 S. Ezrahi, I. Nir, A. Aserin, N. Kozlovich, Y. Feldman and N. Garti, J. Dispersion Sci. Technol., 23 (2002) 351.
23 D. Senatra, Thermochim. Acta, 345 (2000) 39.
24 A. Yaghmur, A. Aserin, I. Tiunova and N. Garti, J. Therm. Anal. Cal., 69 (2002) 163.
25 H. F. Eicke, W. Meier and H. Hammerich, Langmuir, 10 (1994) 2223.
26 S. Ezrahi, E. Wachtel, A. Aserin and N. Garti, J. Colloid Interface Sci., 191 (1997) 277.
27 The Merck Index, Eleventh edition (1989), Merck Co. Inc., Rahway, NJ, USA.
28 C. Stubenrauch and G. H. Findenegg, Langmuir, 14 (1998) 6005.

Received: April 8, 2005
Accepted: June 28, 2005

DOI: 10.1007/s10973-005-7037-5
Online first: December 12, 2005